

# Chaos and Statistical Mechanics in the Hamiltonian Mean Field model

Vito Latora<sup>1</sup>

*Center for Theoretical Physics, Laboratory for Nuclear Sciences and Department of Physics, Massachusetts Institute of Technology, Cambridge, Massachusetts 02139, USA*

Andrea Rapisarda<sup>2</sup>

*Istituto Nazionale di Fisica Nucleare, Sezione di Catania and Dipartimento di Fisica, Università di Catania, Corso Italia 57, I-95129 Catania, Italy*

Stefano Ruffo<sup>3</sup>

*Dipartimento di Energetica "S. Stecco", Università di Firenze, Via S. Marta, 3 I-50139, Firenze, Italy*

---

## Abstract

We study the dynamical and statistical behavior of the Hamiltonian Mean Field (HMF) model in order to investigate the relation between microscopic chaos and phase transitions. HMF is a simple toy model of  $N$  fully-coupled rotators which shows a second order phase transition. The canonical thermodynamical solution is briefly recalled and its predictions are tested numerically at finite  $N$ . The Vlasov stationary solution is shown to give the same consistency equation of the canonical solution and its predictions for rotator angle and momenta distribution functions agree very well with numerical simulations. A link is established between the behavior of the maximal Lyapunov exponent and that of thermodynamical fluctuations, expressed by kinetic energy fluctuations or specific heat. The extensivity of chaos in the  $N \rightarrow \infty$  limit is tested through the scaling properties of Lyapunov spectra and of the Kolmogorov-Sinai entropy. Chaotic dynamics provides the mixing property in phase space necessary for obtaining equilibration; however, the relaxation time to equilibrium grows with  $N$ , at least near the critical point. Our results constitute an interesting bridge between Hamiltonian chaos in many degrees of freedom systems and equilibrium thermodynamics.

*Key words:* Hamiltonian dynamics, equilibrium statistical mechanics, Lyapunov exponents, relaxation to equilibrium

*PACS numbers:* 05.70.Fh, 05.45.+b

---

## 1 Introduction

Many particle systems can show collective behavior when the average kinetic energy is small enough. This collective macroscopic behavior can coexist with chaos at the microscopic level. Such a behavior is particularly evident for systems that have a phase transition, for which a nonvanishing order parameter measures the degree of macroscopic organization, while at the microscopic level chaotic motion is a source of disorder. The latter can induce non trivial time dependence in the macroscopic quantities, and it would be desirable to relate the time behavior of such quantities and their fluctuations to the chaotic properties of microscopic motion, measured through the Lyapunov spectrum. A naive idea is that an increase of chaos as the energy (temperature) is increased should be accompanied with a growth of fluctuations of some macroscopic quantity. These should be maximal at the critical point and then drop again at high energy. In this paper we study a model of  $N$  fully-coupled Hamiltonian rotators which realizes such a behavior, it has been called Hamiltonian Mean Field (HMF) model [1,2]. It can also be considered as a system of interacting particles moving on a circle. This system has a second order phase transition and in the ordered phase the rotators are clustered; the high temperature phase is a gaseous one, with the particles uniformly distributed on the circle. We show that the maximal Lyapunov exponent and the Kolmogorov-Sinai entropy grow up to the critical energy density  $U_c$  and then drop to zero in the whole high temperature phase in the  $N \rightarrow \infty$  limit. Correspondingly one observes a growth of kinetic energy fluctuations (and of specific heat) up to the critical point and then a phase of vanishing fluctuations and constant specific heat. Finite  $N$  effects complicate this simple picture. In the high temperature phase the maximal Lyapunov exponent vanishes quite slowly (with  $N^{-1/3}$ ) and finite size effects influence the first region below the critical point. In this region the system displays metastability: starting far from equilibrium, this is reached in a time  $\tau_r$  which grows with  $N$ . On the contrary, the extremely low energy phase is characterized by a weak  $N$  dependence, with the maximal Lyapunov exponent  $\lambda_1$  which behaves as  $\lambda_1 \sim \sqrt{U}$ . A similar behavior is observed for the Kolmogorov-Sinai entropy per particle  $S_{KS}/N$ , though it scales with different power laws. Although the model is extremely simplified, it shares many features with more complex models, for which the relation between chaotic motion at the microscopic level and collective macroscopic properties has been studied. Let us mention studies in solid state physics and lattice field theory [3–7]. But it has been actually in nuclear physics [8,9], where there is presently a lively debate on multifragmentation phase transition [8–15], that the interest in the connection between chaos and

---

<sup>1</sup> E-mail: latora@ctp.mit.edu

<sup>2</sup> E-mail: andrea.rapisarda@ct.infn.it

<sup>3</sup> and INFN Firenze, E-mail: ruffo@ing.unifi.it

phase transitions has been revived. In this case in fact, an energy/temperature relation quite close to the HMF model has been observed [11] and critical exponents have been measured experimentally [12]. A percolation approach has been proved to give a good description of the experimental data [14], though the dynamics is missing. On the other hand classical molecular dynamic models [9,10,13] seem to contain all the main ingredients, but it can be complicated to understand the dynamics. In this respect, the HMF model can be very useful in clarifying some general dynamical features which could be eventually compared with real experimental data. In fact, when studying nuclear multifragmentation, one deals with excited clusters of 100-200 particles interacting via long-range (nuclear and Coulomb) forces. Quantum effects are relevant only at very low energy, and in fact in the nuclear case, at very low energy,  $T$  is not linear in  $U$ , but grows as  $\sqrt{U}$  [10,11]; however, a classical picture should be quite realistic in the critical region [15].

The paper is organized as follows. In Sec. 2 we briefly discuss the details of the HMF model. The equilibrium statistical mechanics and the continuum Vlasov solution are described in Sects. 3 and 4 respectively. In Sec. 5 we discuss the relaxation to equilibrium and in Sec. 6 we present the numerical calculations of the Lyapunov spectra and Kolmogorov-Sinai entropy as a function of the energy and  $N$ . Analytical estimates are discussed in Sec. 7 and conclusions are drawn in Sec. 8.

## 2 The HMF model

The Hamiltonian we consider is the following

$$H(\{\theta_i\}, \{p_i\}) = K + V, \quad (1)$$

where

$$K = \sum_{i=1}^N \frac{1}{2} p_i^2, \quad V = \frac{\epsilon}{2N} \sum_{i,j=1}^N [1 - \cos(\theta_i - \theta_j)] \quad (2)$$

are the kinetic and potential energies. The model describes the motion of  $N$  rotators characterized by the angle  $\theta_i \in [0, 2\pi)$ : each rotator interacts with all the others. One can define a spin vector associated with each rotator  $\mathbf{m}_i = (\cos(\theta_i), \sin(\theta_i))$ . The Hamiltonian then describes  $N$  classical spins similarly to the XY model, and a ferromagnetic or an antiferromagnetic behavior according to the positive or negative sign of  $\epsilon$  [1]. In the following we will consider only the ferromagnetic (attractive) case and moreover we put  $\epsilon = 1$  without loss of

generality. After defining  $\mathbf{M} = \frac{1}{N} \sum_{i=1}^N \mathbf{m}_i = (M_x, M_y)$ , the potential energy  $V$  can be rewritten as

$$V = \frac{N}{2}(1 - (M_x^2 + M_y^2)) = \frac{N}{2}(1 - M^2) . \quad (3)$$

The equations of motion then read

$$\dot{\theta}_i = p_i \quad , \quad \dot{p}_i = -\sin(\theta_i)M_x + \cos(\theta_i)M_y \quad , \quad i = 1, \dots, N . \quad (4)$$

The evolution equations of the tangent vector are

$$\delta\dot{\theta}_i = \delta p_i \quad , \quad \delta\dot{p}_i = - \sum_j \frac{\partial^2 V}{\partial \theta_i \partial \theta_j} \delta \theta_j \quad , \quad i = 1, \dots, N. \quad (5)$$

where the diagonal and off-diagonal terms of the Jacobian  $J_{ij} = -\partial^2 V / \partial \theta_i \partial \theta_j$  are

$$J_{ii} = -\cos(\theta_i)M_x - \sin(\theta_i)M_y + \frac{1}{N} \quad (6)$$

$$J_{ij} = \frac{1}{N} \cos(\theta_i - \theta_j) \quad , \quad i \neq j . \quad (7)$$

Expression (6) can also be written for convenience as:

$$J_{ii} = -M \cos(\theta_i - \phi) + \frac{1}{N} \quad (8)$$

where  $\phi$  is the phase of  $\mathbf{M}$ .

The HMF model was initially proposed in Ref [1]. A time discrete version of it was previously introduced by Kaneko and Konishi [17] in the form of globally coupled Chirikov standard maps. The Lyapunov instability of the HMF has been first studied numerically by Yamaguchi [6], and analytically by Firpo [18] using the Riemannian geometry approach of Pettini and co-workers [7]. The connection between Lyapunov instability and thermodynamical properties has been established in Ref. [2]. In the original proposal of the HMF [1], the relation of the model with self-gravitating systems (in the attractive case) and charged sheets models (in the repulsive case) was studied; this has been also taken over for the gravitational case by Inagaki [19] and by Elskens and co-workers in the context of plasma models [20]. It has also been shown that the HMF is the peculiar representative of a larger class of models, whose thermodynamics can be solved exactly [21]. Moreover, anomalous diffusion properties of a generalization of the model, with two angles for each rotator, have been studied by Antoni and Torcini [22].

### 3 Canonical and microcanonical results

It is interesting to look at the predictions of statistical mechanics. We restrict here to the  $N \rightarrow \infty$  limit, where microcanonical and canonical ensemble results coincide for averaged quantities (apart from exceptions near first order phase transitions, see Refs. [23]). The free energy of our model can be easily obtained in the canonical ensemble. This was done in Ref. [1] and the result reads

$$-\beta F = \frac{1}{2} \log\left(\frac{2\pi}{\beta}\right) - \frac{\beta}{2} + \max_y \left( -\frac{y^2}{2\beta} + \log(2\pi I_0(y)) \right), \quad (9)$$

where  $\beta = 1/k_B T$  (the Boltzmann constant  $k_B$  is set to 1) and  $I_i$  is the modified Bessel function of  $i$ -th order. The auxiliary variable  $y$  is introduced to decouple the particles by the usual Hubbard-Stratonovich trick for Gaussian integrals, and the search of the maximum in Eq. (9) (which is a consequence of the continuum limit  $N \rightarrow \infty$  solved with the saddle point method) leads to the consistency equation

$$\frac{y}{\beta} - \frac{I_1}{I_0}(y) = 0. \quad (10)$$

The magnetization  $M = I_1/I_0$  is obtained by solving the consistency equation, which is done numerically. It vanishes for  $\beta < \beta_c = 2$ , the inverse critical temperature. At low temperatures it approaches 1 (the limit of  $I_1/I_0$ ).

The energy-temperature relation (sometimes called the *caloric curve*) is

$$U = \frac{E}{N} = \frac{\partial(\beta F)}{\partial \beta} = \frac{1}{2\beta} + \frac{1}{2}(1 - M^2), \quad (11)$$

thus  $U_c = E_c/N = 3/4$ .

Close to the critical point  $\beta \rightarrow \beta_c^+$ , magnetization and energy behave as

$$M \approx \frac{4}{\beta} \sqrt{\frac{1}{2} - \frac{1}{\beta}} \quad (12)$$

$$U \approx \frac{1}{2\beta} \left[ 1 - \frac{8(\beta - 2)}{\beta^2} \right] + \frac{1}{2}. \quad (13)$$

So  $M$  vanishes with the  $1/2$  classical mean field exponent and the specific heat  $C_V = \partial U / \partial T$  is finite at the critical point  $C_V(\beta_c) = 5/2$  and constant ( $C_V = 1/2$ ) in the high temperature phase.

These theoretical results are compared with those of numerical simulations in Fig. 1, where care is taken to use almost equilibrated initial data in order to reduce the relaxation time (as discussed in Sects. 4 and 5). We have integrated Eqs. (4) using fourth order symplectic algorithms [24] with a time step  $\Delta t \sim 0.2$ , adjusted to maintain the error in energy conservation below  $\frac{\Delta E}{E} = 10^{-5}$ . The agreement is good over the whole energy range and finite  $N$  effects, although present, are weak.

In the inset of Fig. 1b we plot the results obtained starting from non equilibrated initial data (the “water bag” initial condition discussed in Sect. 5) and although the integration time was quite long ( $O(10^5)$ ), a sharp disagreement is observed just below the critical point. A region of negative specific heat is present and a continuation of the high temperature phase (linear  $T$  vs.  $U$  relation) into the low temperature one (metastability). It is very intriguing that these out-of-equilibrium quasi-stationary states (QSS) show a caloric curve very similar to the one found for first order phase transitions [22,23,25,26]. In that case, however, the corresponding states are equilibrated and do not die asymptotically, as it is shown in Sec. 5 for our QSS. In our case, at equilibrium, we have not phase-coexistence, all rotators belong to a single cluster (see Sec. 4); phase-coexistence can arise only as a finite  $N$  non-equilibrium effect. The existence of long-living non-equilibrium states has been noticed already in Refs. [2,6] and a connection to critical slowing down has also been proposed. More recently it has also been found numerically in other one-dimensional models [27] and in self-gravitating systems [28], but in this case it is not associated to the closeness of a phase transition. The coexistence of different states in the continuum limit near the critical point is a purely microcanonical effect. It arises because of the inversion of the  $t \rightarrow \infty$  limit with the  $N \rightarrow \infty$  one.

Concerning fluctuations, it is well known that the predictions of microcanonical ensemble differ from those of the canonical [29]. For instance, while in the canonical ensemble kinetic energy fluctuations are given by

$$\Sigma_{can} = \frac{\sigma_{can}(K)}{\sqrt{N}} = \sqrt{\frac{(\langle K^2 \rangle_{can} - \langle K \rangle_{can}^2)}{N}} = \frac{1}{\sqrt{2}\beta}, \quad (14)$$

their expression in the microcanonical ensemble is [18]

$$\Sigma_{\mu} = \frac{\sigma_{\mu}(K)}{\sqrt{N}} = \frac{T_{\mu}}{\sqrt{2}} \sqrt{1 - \frac{1}{1 - 2M(dM/dT_{\mu})}} \quad (15)$$

where  $T_{\mu} = 2 \langle K \rangle_{\mu} / N$  (for a rigorous definition of microcanonical temperature see [30]). The latter is compared with numerical simulations in Fig. 5b.

The specific heat is [29]

$$C_V^\mu = \frac{1}{2} \left( 1 - 2 \left( \frac{\Sigma_\mu}{T_\mu} \right)^2 \right)^{-1}, \quad (16)$$

and also compares quite well with numerical simulations (see Fig. 5c); although finite  $N$  effects are obviously stronger for fluctuations than for the averages.

#### 4 The Vlasov solution

The Vlasov equation for our system reads

$$\frac{\partial f}{\partial t} + p \frac{\partial f}{\partial \theta} - \frac{\partial V}{\partial \theta} \frac{\partial f}{\partial p} = 0, \quad (17)$$

where  $f(\theta, p, t)$  is the normalized distribution function and the potential  $V$  satisfies the equation

$$\frac{\partial^2 V}{\partial \theta^2} = \int_0^{2\pi} \int_{-\infty}^{\infty} \cos(\theta - \theta') f(\theta', p', t) d\theta' dp'. \quad (18)$$

By making the factorization hypothesis

$$f = f_0(p)g(\theta, t) \quad (19)$$

and further requiring that  $f_0$  is Gaussian

$$f_0 = \frac{1}{\sqrt{2\pi T}} \exp -\frac{p^2}{2T}, \quad (20)$$

one gets the equation

$$\frac{\partial g}{\partial t} + p \frac{\partial g}{\partial \theta} - \frac{p}{T} (M_y \cos \theta - M_x \sin \theta) g(\theta) = 0 \quad (21)$$

where  $M_x = \int \cos \theta g d\theta$ ,  $M_y = \int \sin \theta g d\theta$ .

Restricting to the stationary solution,  $\partial g / \partial t = 0$  one can easily solve for  $g(\theta)$

$$g = g_0 \exp \left[ \frac{1}{T} (M_y \sin \theta + M_x \cos \theta) \right] = g_0 \exp \left[ \frac{M}{T} \cos(\theta - \phi) \right], \quad (22)$$

where  $g_0 = 1/(2\pi I_0(M/T))$  as imposed by normalization and  $\phi$  is the phase of  $\mathbf{M}$ . It must be observed that  $g$  is expressed in terms of  $(M_x, M_y)$  or  $(M, \phi)$ , which are themselves functions of  $g$ ; so one must solve the problem self-consistently, after writing the equations for the two components of the magnetization

$$M_x = \cos \phi \frac{I_1(M/T)}{I_0(M/T)} \quad (23)$$

$$M_y = \sin \phi \frac{I_1(M/T)}{I_0(M/T)} . \quad (24)$$

These equations coincide exactly with the consistency equations (10) of the solution in the canonical ensemble. Once  $(M_x, M_y)$  are determined by solving (numerically) Eqs. (23,24), they can be substituted back into Eq.(22), thus obtaining the stationary distribution function. Due to the global phase translation invariance of the model, for any  $M$  the choice of the phase  $\phi$  is arbitrary, as reflected in the solutions of Eqs. (23,24).

In the high temperature phase  $\mathbf{M} = 0$  thus  $g = 1/(2\pi)$  is uniform.

At very low temperature one can use the asymptotic development of  $I_0$

$$I_0(z) = \frac{\exp(z)}{\sqrt{2\pi z}} \left[ 1 + \frac{1}{8z} + \dots \right] \quad (25)$$

to get the Gaussian

$$g \sim \frac{1}{\sqrt{2\pi\sigma^2}} \exp \left( -\frac{\theta^2}{2\sigma^2} \right) , \quad (26)$$

where  $\sigma^2 = T/M$  is the variance, which vanishes with  $T$ , giving a Dirac- $\delta$  at zero temperature.

A comparison of formulas (20,22) with numerical data is shown in Fig. 2; the theoretical curve fits the data very accurately with no free parameter. Both in the low energy region (Fig. 2a,b) and at higher energy, where the cluster drifts (Fig. 2c,d), the agreement is very good. The theory does not determine the value of  $\phi$ , which remains arbitrary; so we have adjusted this value to the center of the cluster, which is moving in time quite irregularly.



## 5 Slow relaxation to equilibrium

Around the critical energy, relaxation to equilibrium depends in a very sensitive way on the adopted initial condition [31]. When starting with “water bag” initial conditions, i.e. a flat distribution function of finite width centered around zero for  $f_0(p)$ , and putting all rotators at  $q_i = 0$  ( $g(\theta) = \delta(0)$ ), we reveal the presence of quasi-stationary (long living) non-equilibrium states (QSS) (see the inset of Fig. 1b). In Fig. 3 the evolution to equilibrium of the QSS state is shown by the time evolution of the reduced distribution function  $f_0(p, t)$ . It is only at  $t = 5 \cdot 10^5$  that a good reproduction of the Gaussian distribution and a convergence to the predicted equilibrium temperature  $T_\mu = 0.4757$  for  $U = 0.69$  is obtained for  $N = 1000$ . Such a slow relaxation is observed in the region just below the critical point (see Fig. 1b) and also around  $U \sim 1$ . In order to study the  $N$ -dependence of the relaxation time  $\tau_r$  we have roughly quantified the distance from the equilibrium state by measuring

$$\Delta S = |S(t) - S^{eq}|, \quad (27)$$

where  $S = - \int f_0(p, t) \ln f_0(p, t) dp$  is the Boltzmann entropy of the momentum reduced distribution function, and  $S^{eq}$  its equilibrium value when the distribution is a Gaussian at the given equilibrium temperature  $T_\mu$ . The results, shown in Fig. 4, clearly indicate an increase of the relaxation time with  $N$  (Fig. 4(a)), which can be approximately fitted with a linear law  $\tau_r \sim N$ . The convergence to the equilibrium value of  $S$  is not exact at finite  $N$  and the error decreases as  $N^{-1/2}$ ; this is shown in Fig. 4(a) by the convergence to a decreasing value (horizontal lines) as  $N$  is increased from 1000 to 10000. A similar law was found in Ref. [1] by studying the time needed to reach equipartition of rotators velocity in the large  $U$  region and in Ref. [21] analysing the time needed to absorb holes in the momentum distribution (so called Dupree structures in plasma physics) for the antiferromagnetic HMF. It then seems that various indicators agree in suggesting a diverging time scale with  $N$ . However, the time scale also depends on  $U$ , and what we have here found is that it is much greater in the region near the critical point. This could be a manifestation of critical slowing down.

## 6 Lyapunov spectra and Kolmogorov-Sinai Entropy

We have computed the Lyapunov spectrum  $\lambda_i$ ,  $i = 1, \dots, N$  by the standard method of Ref. [32]. The average number of time steps in order to get a good convergence was of the order  $10^6$ . We discuss in the following numerical results for system sizes in between  $N=10$  and  $N=20000$ .

In Fig. 5(a) we plot  $\lambda_1$  as a function of  $U$  for various  $N$  values. Being the system integrable both in the limit of very small and very large energies (reducing in the former case to weakly coupled harmonic oscillators and in the latter to free rotators), the maximal Lyapunov exponent must vanish in these two limits.

In the region of weak chaos, for  $U < 0.25$ , the curve has a weak  $N$ -dependence. Then  $\lambda_1$  changes abruptly and a region of stronger chaos begins. In Ref. [1] it was observed that in between  $U = 0.2$  and  $U = 0.3$  a different dynamical regime sets in and particles start to evaporate from the main cluster. A similar regime was found in Ref. [9] and this behavior is also similar to the one found in Ref. [4] at a solid-liquid transition. In this region of strong chaoticity we observe a pronounced peak already for  $N = 100$  [6], which persists and becomes broader for  $N = 20000$ .

The standard deviation  $\Sigma_\mu$  of the kinetic energy fluctuations is plotted in Fig. 5(b) and it compares quite well with the theoretical prediction (15), although finite  $N$  effects are larger than for averaged quantities. In Fig. 5(c) we report the microcanonical specific heat obtained with formula (16), compared with numerical simulations at increasing values of  $N$ . Both these quantities display a similar behavior to the maximal Lyapunov exponent: they increase up to the critical point and then drop to zero. It is therefore quite natural to associate the growth of the Lyapunov exponent to the growth of fluctuations, as expressed both by the kinetic energy fluctuations and the specific heat. In this respect a similar connection was proposed in Ref. [16]. Unfortunately, a theoretical formula for the Lyapunov exponent as  $N \rightarrow \infty$  does not yet exist (see anyway next section); however, the data in Fig. 5(a) already show what we should expect for the convergence of  $\lambda_1$  as  $N$  increases. For  $U \geq U_c$ ,  $\lambda_1 \rightarrow 0$  as  $N \rightarrow \infty$ , thus revealing the presence of a whole region of integrability in this limit; rotators decouple, reducing the system to a “gas” of free rotators (which is consistent also with the vanishing of kinetic energy fluctuations). Fig. 6(a) shows that the convergence to zero can be fitted as  $\lambda_1 \sim N^{-1/3}$ . This scaling law can be derived theoretically using a random matrix approximation [2] (see also next section), which is also shown in the same figure to approximate quite well the numerical results at large enough energy. (A  $N^{-1/3}$  convergence to the asymptotic value of the Lyapunov exponent is also observed in systems of hard spheres [33]). The question is still open whether  $\lambda_1$  will show a discontinuity at  $U_c$  in the  $N \rightarrow \infty$  limit, as the kinetic energy fluctuations and specific heat do. Strong finite size effects are present in the region  $U \in [0.2, 0.75]$ . This is the region where the cluster drifts (see [1]), while particles evaporate from and condensate on it. The Lyapunov exponent is here significantly larger than at smaller energies. For  $U < 0.2$ , we observe a fast convergence to the  $N \rightarrow \infty$  limit, and the scaling law  $\lambda_1 \sim \sqrt{U}$  is numerically obtained (see Fig. 6(b)). A heuristic justification of this scaling was proposed in Ref. [2], and a new derivation is presented in Sec. 7.1.

The extensivity of the Lyapunov spectrum was first proposed by Ruelle [34] and numerically tested in Refs. [35] (see [36] for a review). It amounts to check that plotting  $\lambda_i$  vs.  $i/N$  and letting  $N$  go to infinity, while keeping fixed physically intensive parameters (in our case energy density or temperature), one obtains a convergence to an asymptotic curve, so called distribution of Lyapunov exponent. This is verified for our model in Fig. 7(a) at various energy densities. The asymptotic Lyapunov distribution is more quickly reached, as  $N$  increases, at smaller energies (confirming the fast  $N$  convergence observed above for the maximal Lyapunov exponent at small energy). The spectra have a curious exponential shape in the first part (see the inset of Fig. 7(a)), which was already noticed in Ref. [17]. No significative change in the shape of the spectra is observed when going from below to above the phase transition point (see Fig. 7(b)).

The Kolmogorov-Sinai (K-S) entropy density (which, due to Pesin's formula, is in our case the sum of the positive Lyapunov exponents divided by  $N$ ),  $S_{KS}/N$ , is plotted in Fig. 8 against  $U$ . It shows again a peak at  $U_c$ , a fast convergence to a limiting value as  $N$  increases in the small energy limit and a slow convergence to zero (as expected) for  $U \geq U_c$ . The scaling laws are here roughly:  $S_{KS}/N \sim U^{3/4}$  at small  $U$ , see Fig. 9(a), and  $S_{KS}/N \sim N^{-1/5}$  for  $U > U_c$ , see Fig. 9(b) (but a more refined numerical analysis is needed to confirm these results).

Therefore, the analysis of the behavior of the Lyapunov spectrum and of the K-S entropy confirms the picture already emerging from the study of the maximal Lyapunov exponent, showing an increase of microscopic chaos near the phase transition point. It is somewhat intriguing that it is precisely when chaos is stronger that one reveals a slowing down of the relaxation to equilibrium (see Sec. 5); although not unexpected, because it is quite simplistic to associate the notion of chaos to that of efficient diffusion of orbits in phase space. When starting from a “water bag” initial condition one reaches the almost frozen QSS state, and also for this state the transient Lyapunov exponent has been checked to be positive, although slightly different than the asymptotic value in the equilibrium state. It could be that the phase space near the transition point has a rich structure with many coexisting chaotic QSS states.

## 7 Analytical estimates of the maximal Lyapunov exponent

In this section we discuss some theoretical approaches which allow to justify the scaling laws of the maximal Lyapunov exponent observed in numerical experiments, and also to obtain some order of magnitude estimates.

### 7.1 Using the Vlasov solution

One can try to use the stationary Vlasov distribution function (20,22) to derive some properties of the tangent space. For instance, averaging the Jacobian  $J_{ij}$  (6,7) over this distribution, one obtains a constant matrix whose diagonal and off-diagonal elements are  $-M^2+1/N$  and  $M^2/N$ , respectively (we are here also neglecting correlations among the particles). It is then quite easy, being now the Jacobian a constant matrix, to compute the maximal Lyapunov exponent. The result is

$$\lambda_1 = \sqrt{\frac{1-M^2}{N}}, \quad (28)$$

with Lyapunov eigenvector  $(\{\delta\theta_i\}, \{\delta p_i\}) = (\mathbf{a}, \mathbf{b})$ , the vectors  $\mathbf{a}$  and  $\mathbf{b}$  being constant. This formula has the correct dependence on  $M$ , in fact at small energies the virial relation  $\langle K \rangle \sim \langle V \rangle$  holds and then  $U = E/N \sim 1 - M^2$ , giving  $\lambda_1 \sim \sqrt{U}$ , which is what is observed numerically. However, formula (28) predicts that the Lyapunov exponent vanishes with  $N^{-1/2}$ , which is not observed in numerical experiments. We have found numerically that, even if we allow for the true temporal fluctuations of  $M^2$ , we obtain for the Lyapunov exponent the same value of formula (28) and the same Lyapunov eigenvector. On the contrary, if we look at the Lyapunov eigenvector given by the true dynamics, we observe that it is far from being constant, only a few components being significantly different from zero. We have checked that the number of nonvanishing components of the Lyapunov eigenvector remains constant as  $N$  increases, thus the typical size of each component of the vector remains constant as  $N$  grows (remember that eigenvectors are normalized), while for constant eigenvectors this size decreases as  $N^{-1/2}$ ; this can explain the extra  $N^{-1/2}$  present in formula (28) with respect to what is observed for the true Lyapunov, giving then the correct scaling law for the maximal Lyapunov exponent as  $U \rightarrow 0$ , i.e.  $\lambda_1 \sim \sqrt{U}$ .

### 7.2 A numerical test of a recently proposed formula

We compare in this subsection a recently proposed formula for the maximal Lyapunov exponent [7,18] with numerical results, giving also an intuitive interpretation of it for our model. In Ref. [7] Pettini and co-workers formulate a general method to describe Hamiltonian chaos using the differential geometric structure underlying the dynamics. They consider the Hamiltonian many-body dynamics as a geodesic flow on a Riemannian manifold; then the chaotic motion reflects the instabilities of the geodesic flow, which depend on the curvature properties of the manifold. They obtain the following formula

for  $\lambda_1$

$$\lambda_1 = \frac{\Lambda}{2} - \frac{2\Omega_0}{3\Lambda} \ ; \quad \Lambda = \left( 2\sigma_\Omega^2\tau + \sqrt{\left(\frac{4\Omega_0}{3}\right)^3 + (2\sigma_\Omega^2\tau)^2} \right)^{\frac{1}{3}} \ , \quad (29)$$

where  $\Omega_0$  and  $\sigma_\Omega^2$  are the average Ricci curvature and the variance of its fluctuations respectively. For the HMF, these two quantities turn out to be given by very simple expressions in terms of the averages and fluctuations introduced in Sec. 3 (see also ref. [18])

$$\begin{aligned} \Omega_0 &= \langle M^2 \rangle - \frac{1}{N} = T_\mu + (1 - 2U) - \frac{1}{N} \\ \sigma_\Omega^2 &= N\sigma_{M^2}^2 = 4\Sigma_\mu^2 \ , \end{aligned} \quad (30)$$

where  $\sigma_{M^2}^2$  is the variance of the fluctuations of  $M^2$ . All this is the consequence of the fact that the Ricci curvature,  $-1/N \sum_i J_{ii}$  with  $J_{ii}$  given by formula (6), is simply given in our model by  $M^2 - 1/N$ . The Ricci curvature is assumed in Ref. [7] to be a  $\delta$ -correlated stochastic process in time, and the correlation time  $\tau$  in formula (29) is estimated as

$$\tau^{-1} = 2(\tau_1^{-1} + \tau_2^{-1}) \ ; \quad \tau_1 = \frac{\pi}{2\sqrt{\Omega_0 + \sigma_\Omega}} \ ; \quad \tau_2 = \frac{\sqrt{\Omega_0}}{\sigma_\Omega} \quad (31)$$

Some comments about the derivation and the use of formula (29) are very important. It is derived in the “diagonal” approximation, which corresponds to neglect the effect of off-diagonal terms (7) in Eqs. (5). This approximation has been checked numerically not to be valid at small energies, leading to a value of  $\lambda_1$  which is orders of magnitude less than the true one (see also Fig. 10). The assumption of a  $\delta$ -correlated stochastic process makes easier the calculation of  $\lambda_1$ , but reduces the range of applicability of formula (29). The estimate for  $\tau$  is a rather delicate problem, where some arbitrariness can enter the theory [37].

In the high energy phase,  $M$  fluctuates above zero and scales with  $N^{-1/2}$  at large  $N$ , then we have  $\langle M^2 \rangle \sim \sigma_{M^2} \sim N^{-1}$  and moreover  $\tau \approx \tau_2/2$  since  $\tau_2 = M/(\sigma_{M^2}\sqrt{N}) = O(1)$  while  $\tau_1 \sim N^{1/4}$ . Hence one finds [18]

$$\lambda_1 \sim \Lambda \sim (4N\sigma_{M^2}^2\tau)^{1/3} \sim N^{-1/3} \ . \quad (32)$$

In the low energy phase  $\sigma_{M^2} \ll M^2$  and  $\lambda_1$  reduces to

$$\lambda_1 \sim \frac{4\Sigma_\mu^2\tau}{M^2} \quad (33)$$

which gives a relation between  $\lambda_1$  and the fluctuations of kinetic energy. This result support the link between chaos and kinetic energy fluctuations already claimed in Ref.[2] although the formula derived heuristically there was different, but in better agreement with the scaling law for small  $U$ .

In Fig. 10 we compare the numerically computed values of  $\lambda_1$  at increasing values of  $N$  with those obtained from formula (29), using the numerical values of  $\langle M^2 \rangle$  and  $\Sigma_\mu$ . We have also checked that eqs. (30) are well reproduced by numerical simulations. Formula (29) reproduces the behavior of  $\lambda_1$  vs.  $U$  within a factor of two over a large range of energies. In particular it predicts correctly a maximum of  $\lambda_1$  around  $U_c$ .

However, in the limit  $U \rightarrow 0$  this formula gives  $\lambda_1 \sim U^2$ , as can be easily derived from formula (33), which is sharply in contrast with the behaviour  $\lambda_1 \sim \sqrt{U}$  observed in numerical simulations (see Fig. 6(b)). We think that, in this limit, the stochastic approximation for the average Ricci curvature breaks down, because this quantity is in our case nothing but  $M^2$ , and this is an almost regularly oscillating quantity as  $U \rightarrow 0$ , due to the collective excitations of the cluster. However, it is possible to use  $\tau$  as a fitting parameter to reproduce the numerical data. In fact some preliminary numerical investigations have shown that in this region the correlation time given by eq. (31) strongly underestimates the realistic one.

## 8 CONCLUSIONS

We have investigated the dynamical and statistical behavior of a system with long-range forces showing a second order phase transition. Both the maximal Lyapunov exponent  $\lambda_1$  and the Kolmogorov-Sinai entropy density  $S_{KS}/N$  are peaked at the phase transition point, where kinetic energy fluctuations and specific heat are maximal. There is actually a small shift to lower energies due to finite size effects. The latter are present also in the Lyapunov spectra and in the Kolmogorov-Sinai entropy. Above the phase transition point, both  $\lambda_1$  and  $S_{KS}$  vanish as  $N \rightarrow \infty$ . We think that this toy model contains some important ingredients to understand the behavior of macroscopic order parameters when dynamical chaos is present at the microscopic level. Most of our findings are probably common to other Hamiltonian systems showing second order phase transitions. It is very exciting that some of our predictions could be very important in order to understand realistic experiments such as in nuclear multifragmentation reactions.

## Acknowledgements

We thank M.C. Firpo for communicating us her results before publication and P. Holdsworth for interesting suggestions. We thank A. Torcini for many useful discussions and a careful reading of the text. A.R. thanks the Centre for Theoretical Physics of MIT for the kind hospitality and M. Robnik for stimulating discussions during his visits at CAMTP in Maribor. V.L. and S.R. thank INFN for financial support. S.R. thanks CIC, Cuernavaca, Mexico for financial support. This work is also part of the European contract No. ERBCHRXCT940460 on “Stability and universality in classical mechanics”.

*In the 60's, Boris Chirikov was also an explorer of the (no man's land at that time) relation between chaotic motion and statistical behavior in classical systems with many degrees of freedom. We hope that he will be interested by this work.*

## References

- [1] S. Ruffo, in *Transport and Plasma Physics*, S. Benkadda, Y. Elskens and F. Doveil eds., World Scientific, Singapore (1994), p. 114; M. Antoni and S. Ruffo, *Phys. Rev.* **E52**, 2361 (1995).
- [2] V. Latora, A. Rapisarda and S. Ruffo, *Phys. Rev. Lett.* **80**, 692 (1998).
- [3] P. Butera and G. Caravati, *Phys. Rev.* **A36**, 962 (1987); R.J. Hinde, R.S. Berry and D.J. Whales, *J. Chem. Phys.* **96**, 1376 (1992).
- [4] S.K. Nayak, R. Ramaswamy and C. Chakravarty, *Phys. Rev.* **E 51**, 3376 (1995); V. Mehra, R. Ramaswamy, *Phys. Rev.* **E 56**, 2508 (1997).
- [5] Ch. Dellago, H.A. Posch and W.G. Hoover *Phys. Rev.* **E 53** 1485 (1996); Ch. Dellago and H.A. Posch *Physica* **A230**, 364 (1996).
- [6] Y.Y. Yamaguchi, *Progr. of Theor. Phys.* **95** , 717 (1996); Y.Y. Yamaguchi, *J. Phys. A* **31**, 195 (1998).
- [7] L. Casetti, R. Livi and M. Pettini, *Phys. Rev. Lett.* **74** 375, (1995); L. Casetti, C. Clementi and M. Pettini, *Phys. Rev.* **E54**, 5969 (1996); L. Caiani, L. Casetti, C. Clementi and M. Pettini, *Phys. Rev. Lett.* **79** 4361 (1997); L. Caiani, L. Casetti, C. Clementi, G. Pettini, M. Pettini and R. Gatto, LANL preprint hep-th/9706081, *Phys. Rev.* **E57**, (1998) in press.
- [8] G.F. Burgio, M. Baldo and A. Rapisarda *Phys. Lett.* **B321**, 307 (1994); M. Baldo, G.F. Burgio and A. Rapisarda *Phys. Rev.* **C51**, 198 (1995); A. Atalmi, M. Baldo, G.F. Burgio and A. Rapisarda *Phys. Rev.* **C53**, 2556 (1996) A. Atalmi, M. Baldo, G.F. Burgio and A. Rapisarda *Phys. Rev.* **C53**, 2556 (1996)

- and Ref. [10], p.56; B. Jacquot, A. Guarnera, Ph. Chomaz and M. Colonna, *Phys. Rev.* **C54**, 3025 (1997).
- [9] A. Bonasera, V. Latora and A. Rapisarda *Phys. Rev. Lett.* **75**, 3434 (1995).
  - [10] For an up-to-date review see for example: Procs. of the Intern. Conf. CRIS 96, Eds. S. Costa, S. Albergo, A. Insolia and C. Tuvé, World scientific 1996, and refs. therein.
  - [11] J. Pochodzalla et al., *Phys. Rev. Lett.* **75**, 1040 (1995).
  - [12] M.L. Gilkes et al., *Phys. Rev. Lett.* **73**, 1590 (1994).
  - [13] V. Latora, M. Belkacem, and A. Bonasera *Phys. Rev. Lett.* **73**, 1765 (1994); M. Belkacem, V. Latora and A. Bonasera, *Phys. Rev.* **C52**, 271 (1995); P. Finocchiaro et al. *Nucl. Phys.* **A 572**, 477 (1996).
  - [14] X. Campi, *J. Phys.* **A**, L917 (1986); X. Campi, *Phys. Lett.* **B 208**, 351 (1988); W. Bauer, *Phys. Rev.* **C 38**, 1297 (1988); W. Bauer in Ref. [10], p.23 and Refs. therein.
  - [15] P.F. Mastinu et al., *Phys. Rev. Lett.* **76**, 2646 (1996); M. Belkacem et al., *Phys. Rev.* **C54**, 2435 (1996).
  - [16] A. Bonasera, V. Latora and M. Ploszajczak, Ganil preprint No. p9621.
  - [17] K. Kaneko and T. Konishi, *J. Phys. A* **25**, 6283 (1992).
  - [18] M. C. Firpo, *Phys. Rev. E*, in press (1998).
  - [19] S. Inagaki, *Prog. Theor. Phys.* **90**, 577 (1993); S. Inagaki and T. Konishi, *Publ. Astron. Soc. Japan* **45**, 733 (1993).
  - [20] Y. Elskens and M. Antoni, *Phys. Rev. E* **55**, 6575 (1997).
  - [21] M. Antoni, Y. Elskens and C. Sandoz, *Phys. Rev. E*, in press (1998).
  - [22] M. Antoni and A. Torcini, *Phys. Rev. E*, in press (1998).
  - [23] P. Hertel and W. Thirring, *Ann. of Phys.* **63**, 520 (1971); A. Compagner, C. Bruin and A. Roelse, *Phys. Rev.* **A 39**, 5989 (1989).
  - [24] H. Yoshida *Phys. Lett.* **A 150**, 262 (1990); I. McLachlan and P. Atela, *Nonlinearity* **5**, 541 (1992).
  - [25] P. Labastie and R.L. Whetten, *Phys. Rev. Lett.* **65**, 1568 (1990).
  - [26] D.H.E. Gross, A. Ecker and X.Z. Zhang, *Ann. of Phys.* **5**, 446 (1996).
  - [27] Lj. Milanovic, H.A. Posch and W. Thirring, *Phys. Rev. E*, in press (1998).
  - [28] K.R. Yawn and B.N. Miller, *Phys. Rev. Lett.* **79**, 3561 (1997).
  - [29] J.L. Lebowitz, J. K. Percus and L. Verlet, *Phys. Rev.*, **153**, 250 (1967).



- [30] H.H. Rugh, *Phys. Rev. Lett.* **78**, 772 (1997). The temperature defined through the kinetic energy is found in our model to agree with Rugh's temperature.
- [31] M. Antoni, private communication.
- [32] G. Benettin, L. Galgani, A. Giorgilli and J.M. Strelcyn, *Meccanica* **9**, 21 (1980); I. Shimada and T. Nagashima, *Prog. Theor. Phys.* **61** 1605 (1979).
- [33] Ch. Dellago and H.A. Posch, *Physica A* **240**, 68 (1997).
- [34] D. Ruelle, *Commun. Math. Phys.*, **87**, 287 (1982).
- [35] P. Manneville, in *Macroscopic Modeling of Turbulent Flows*, O. Pironneau ed., Lecture Notes in Physics **230**, 319, Springer-Verlag, Berlin (1985); R. Livi, A. Politi and S. Ruffo, *J. Phys. A* **19**, 2033 (1986).
- [36] S. Ruffo in *Fiesta 96, V Escuela del Verano en Sistemas Complejos*, E. Goles and S. Martinez eds., Kluwer, to be published (1998).
- [37] See also Mehra et al. in Ref.[4]

Fig. 1. Theoretical predictions in the canonical ensemble (full curve) for the magnetization  $M$  vs.  $U$ , panel (a), and for the caloric curve  $T$  vs.  $U$ , panel (b), in comparison with numerical simulations (microcanonical ensemble) for  $N=100, 1000, 5000, 20000$ . The vertical line indicates the critical energy  $U_c = 3/4$ . We plot also the microcanonical results for the Quasi-Stationary States (QSS) in the case  $N=20000$  (losanges) in the inset of panel (b).

Fig. 2. Equilibrium reduced distribution functions in angles  $\theta$  and momenta  $p$  for  $U = 0.095$  ((a) and (b)) and  $U = 0.36$  ((c) and (d)). The numerical simulations for  $N = 1000$  (histogram) are compared with the theoretical distributions (20,22)

Fig. 3. Reduced distribution function in  $p$  for  $U = 0.69$  and  $N = 1000$  at increasing times. The initial distribution is a water bag (histogram). The thick full line is the equilibrium distribution.

Fig. 4. (a) Relaxation to equilibrium of the Boltzmann entropy of the reduced distribution in  $p$  for  $N=1000$  and  $N=5000$ ; (b) Linear increase with  $N$  of the time scale  $\tau_r$  for the relaxation to equilibrium

Fig. 5. (a) Numerical data for the largest Lyapunov exponent as a function of  $U$  for various system sizes:  $N=100, 1000, 5000$  and  $20000$ . (b) Kinetic energy fluctuations  $\Sigma_\mu$  vs.  $U$ . (c) Specific heat obtained from formula (16). The vertical line indicates the critical energy  $U_c = 3/4$ . The full lines in panels (b) and (c) are the microcanonical predictions.

Fig. 6. (a) Convergence to zero of the largest Lyapunov exponent vs.  $N$  in the high energy region. The fitted curve is the power law  $N^{-1/3}$ , the circles are the result of a random matrix simulation. (b)  $U^{1/2}$  growth of the maximal Lyapunov exponent vs.  $U$  at small  $U$ , a rather weak  $N$  dependence is observed.

Fig. 7. (a) Lyapunov spectra for three different values of  $U$  at different  $N$  in linear and lin-log scale (inset for  $N = 20$ ) showing the convergence to the asymptotic distribution. (b) Lyapunov spectra for fixed  $N$  with two different values of the energy, below and above the critical energy.

Fig. 8. The Kolmogorov-Sinai entropy density  $S_{KS}/N$  vs.  $U$  at increasing values of  $N$ .

Fig. 9. (a) Growth of the K-S entropy density at small  $U$  with the exponent  $3/4$ . A rather weak  $N$ -dependence is observed. (b) Convergence to zero of the K-S entropy density as  $N$  increases in the high energy region. The fitted curve is the power law  $N^{-1/5}$ .

Fig. 10. Comparison of formula (29) for  $\lambda_1$  (full line) with numerical simulations (circles) at increasing values of  $N$ .

Fig.1

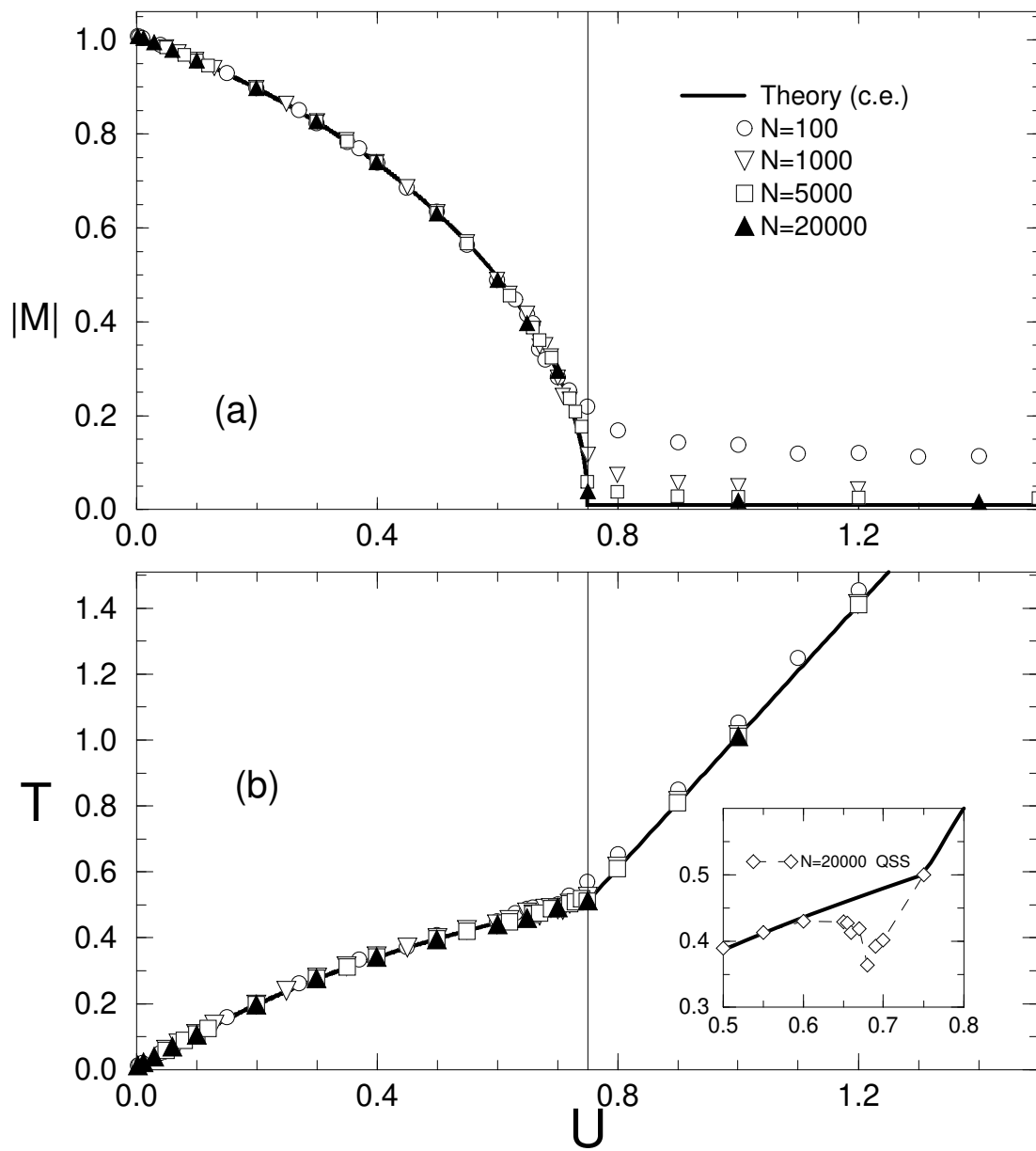


Fig. 2

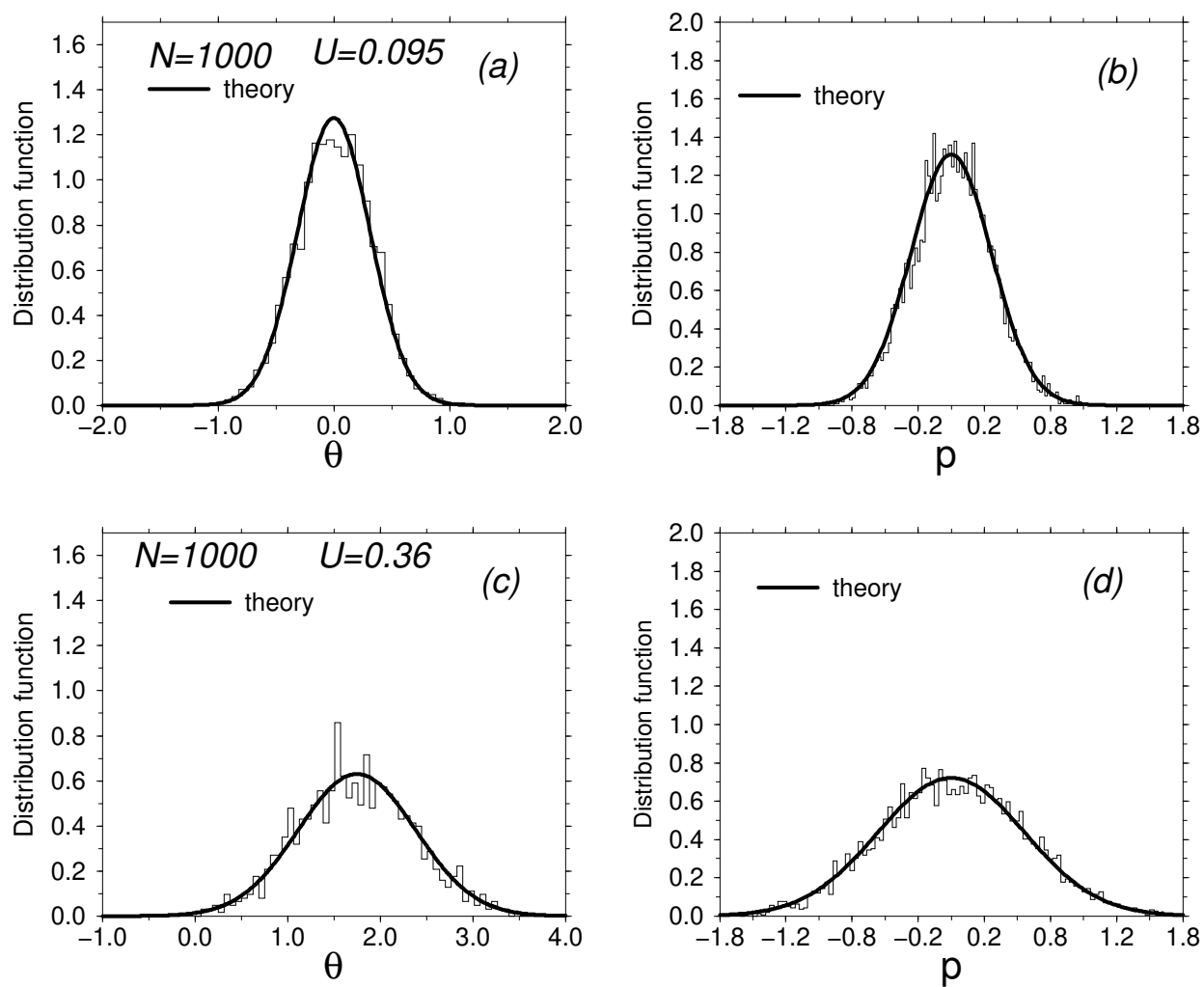


Fig. 3

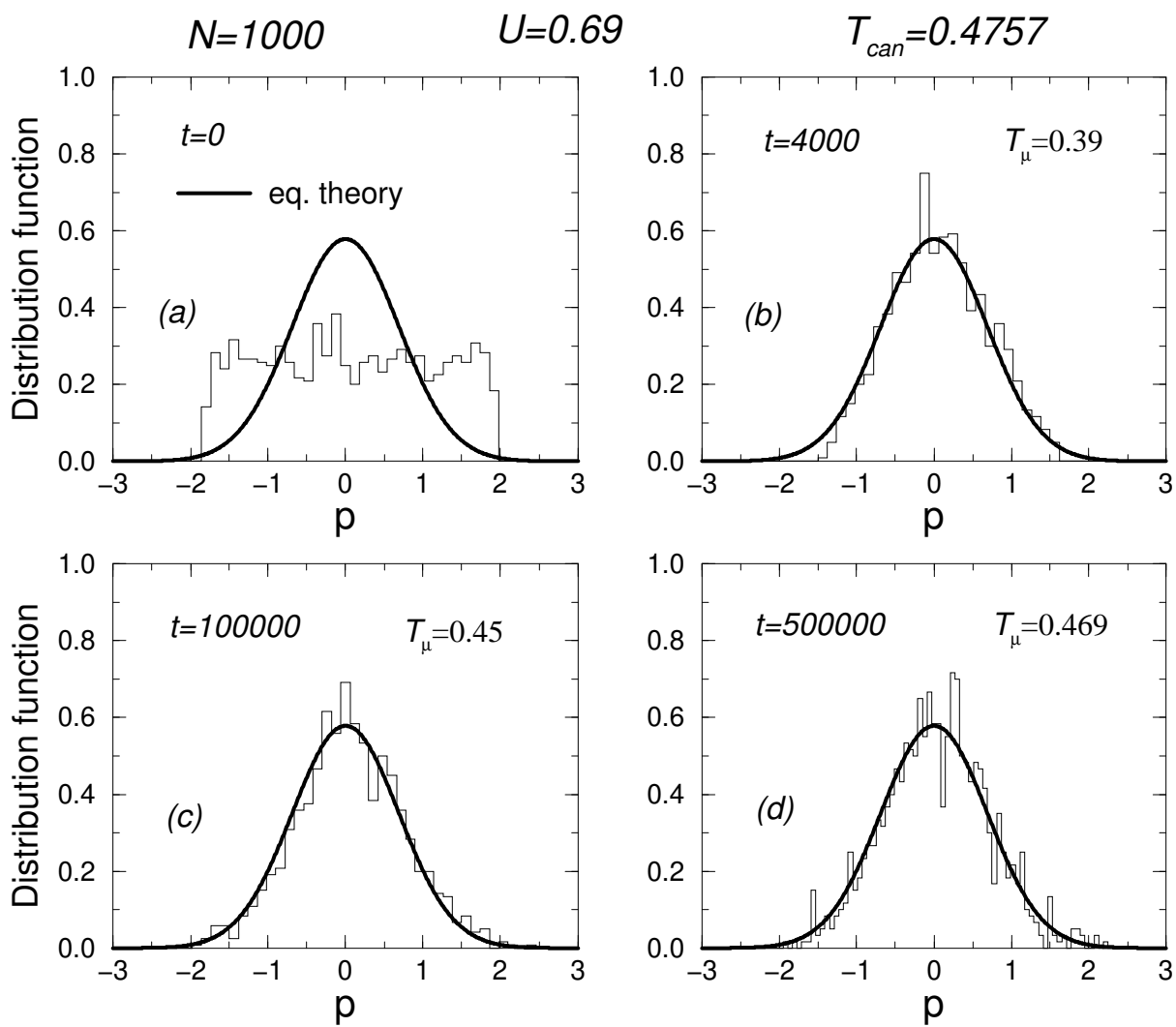


Fig. 4

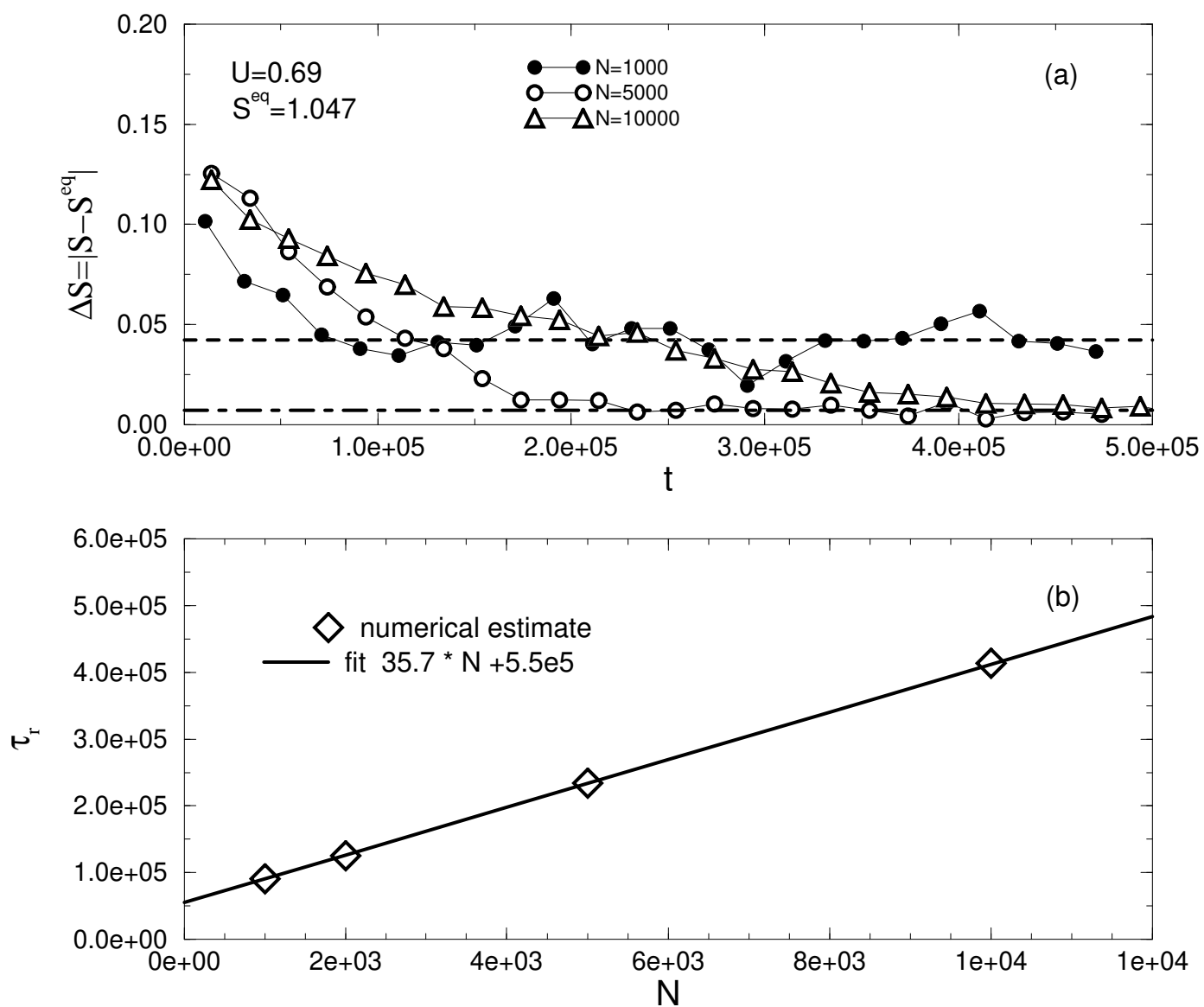


Fig. 5

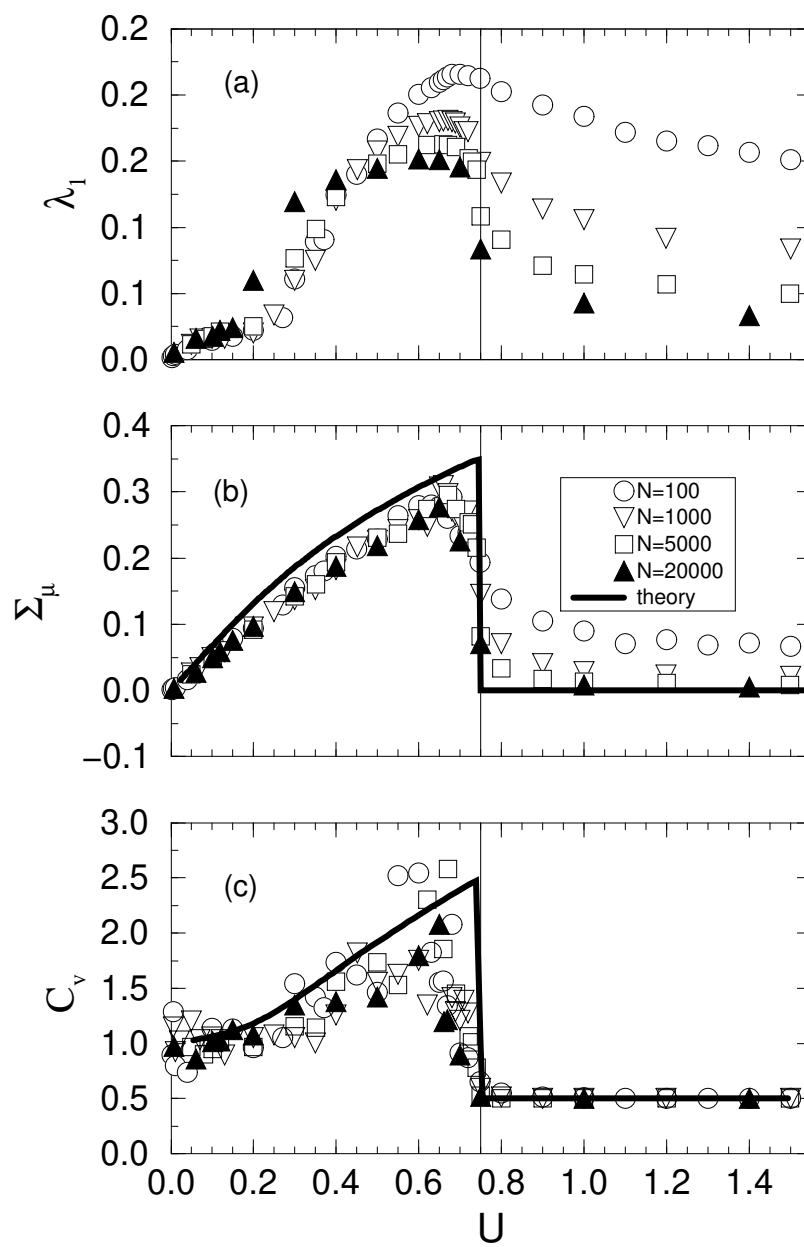


Fig. 6

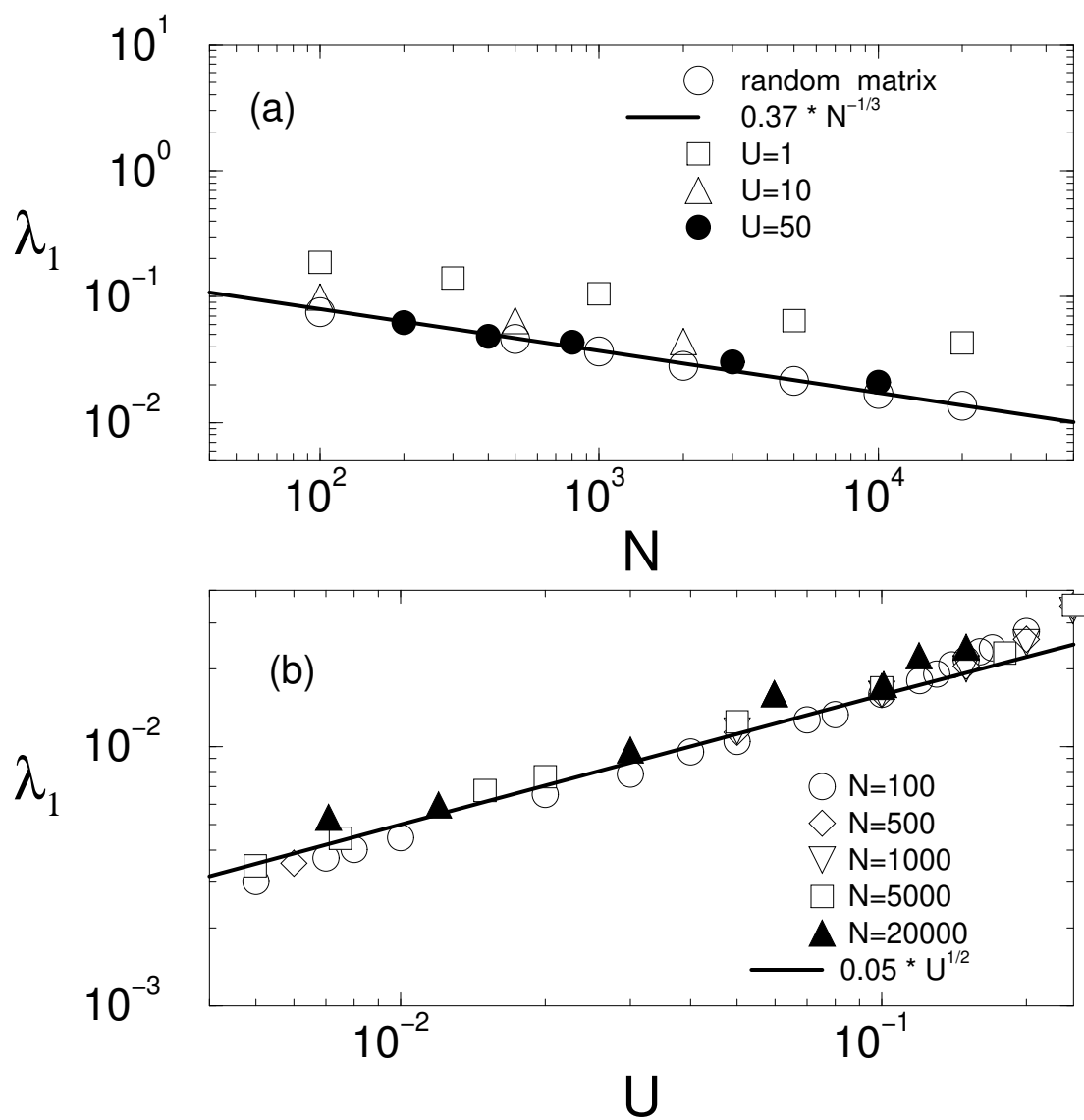




Fig. 7 (a)

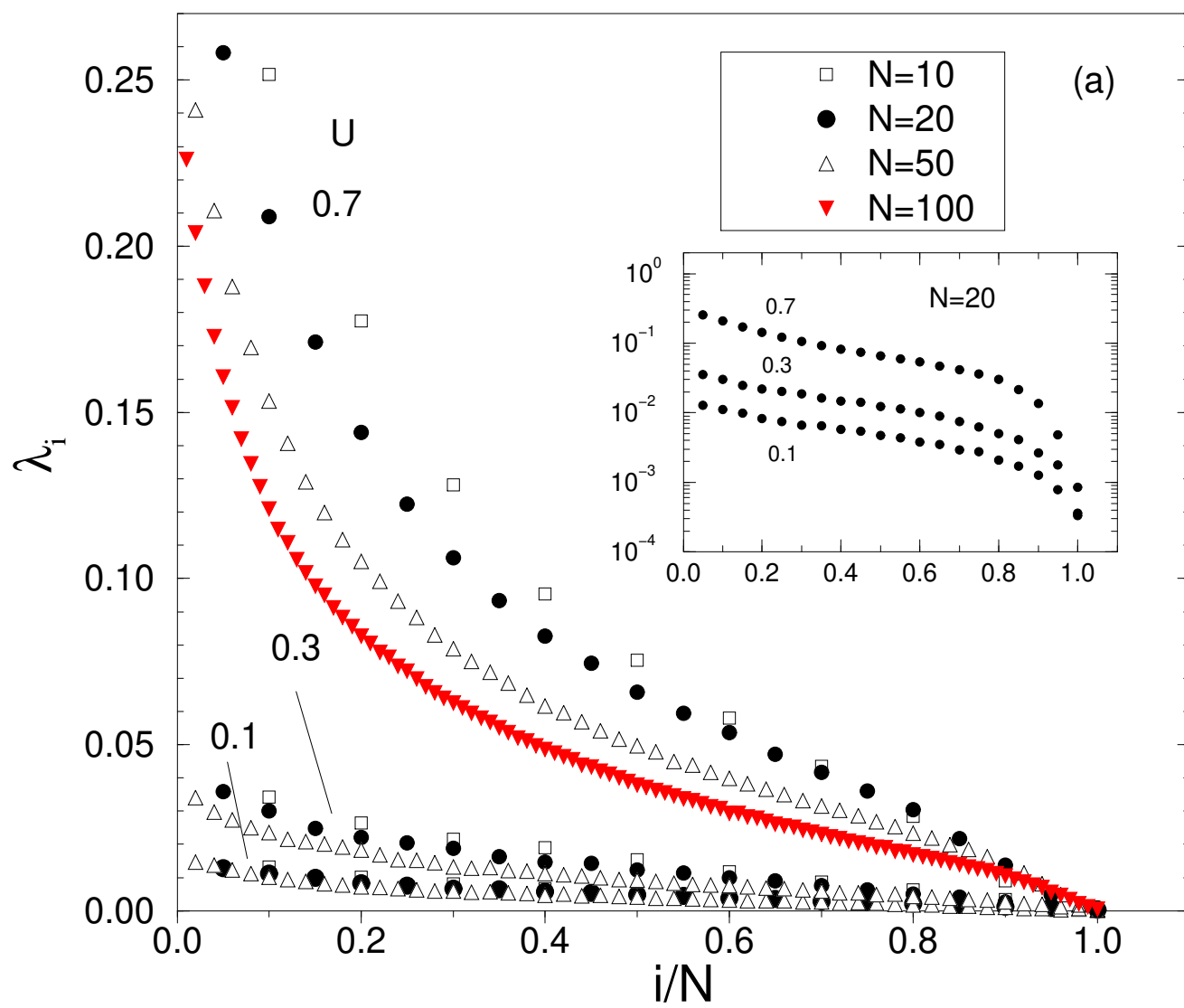


Fig. 7 (b)

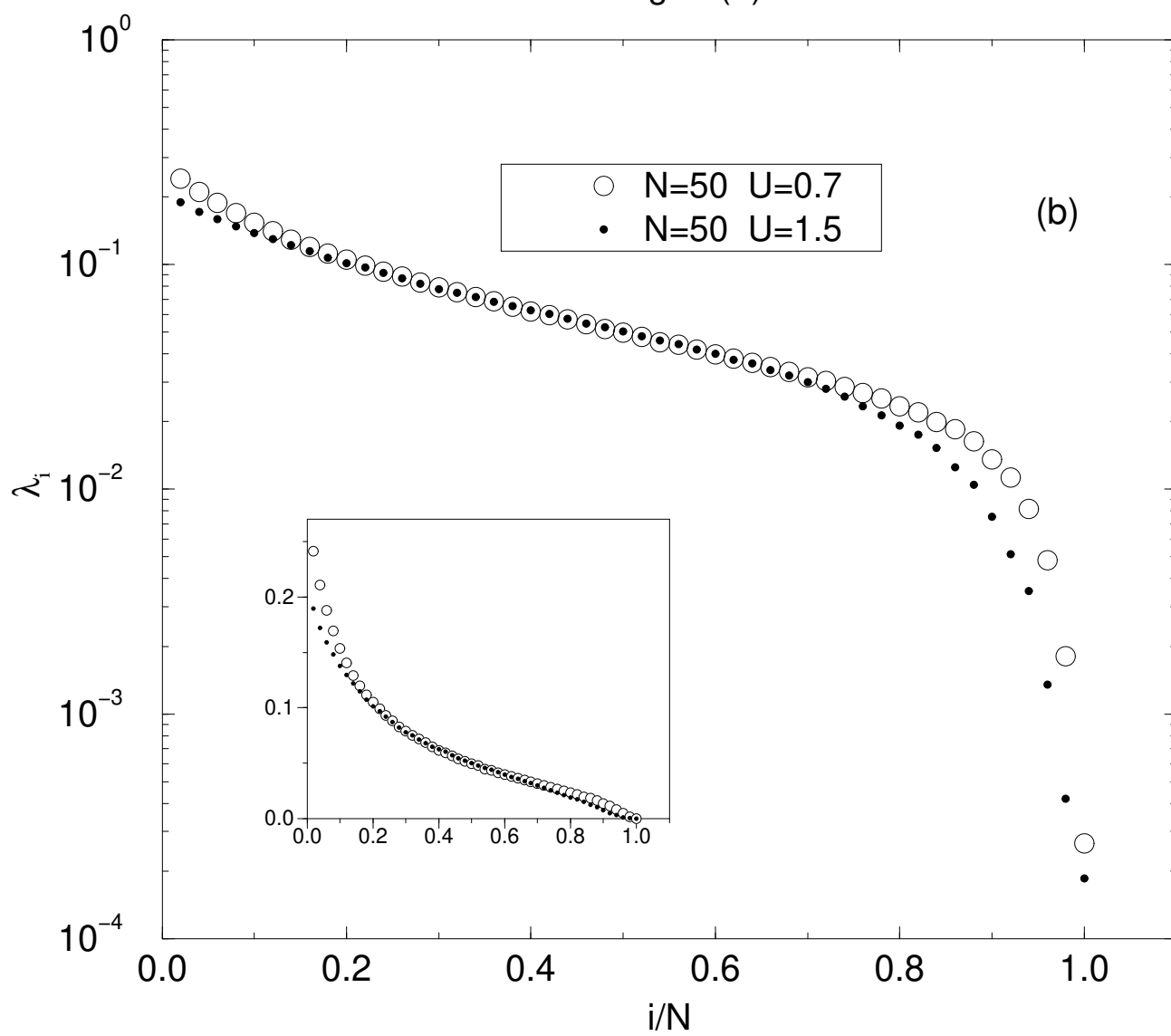


Fig. 8

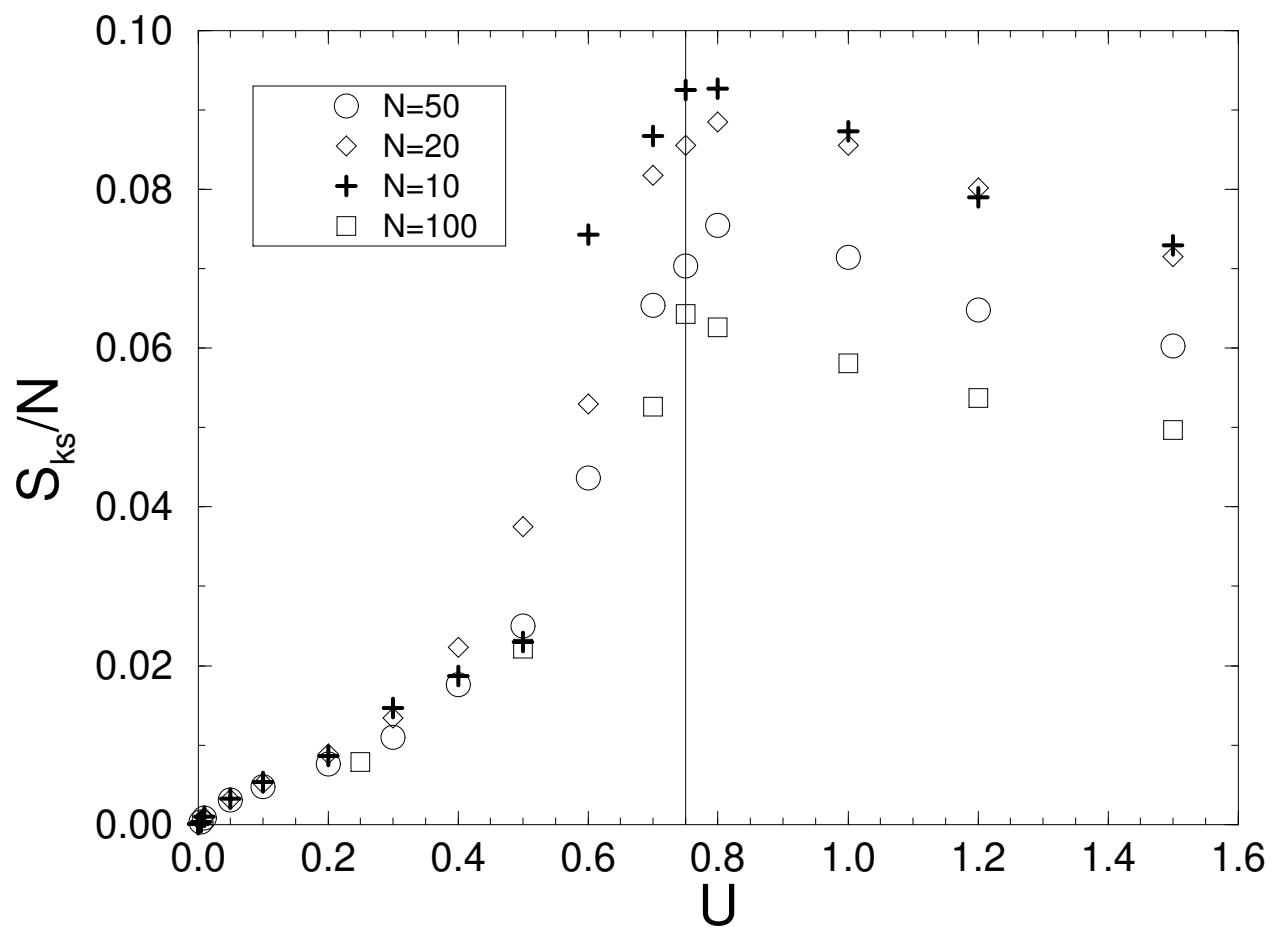


Fig. 9

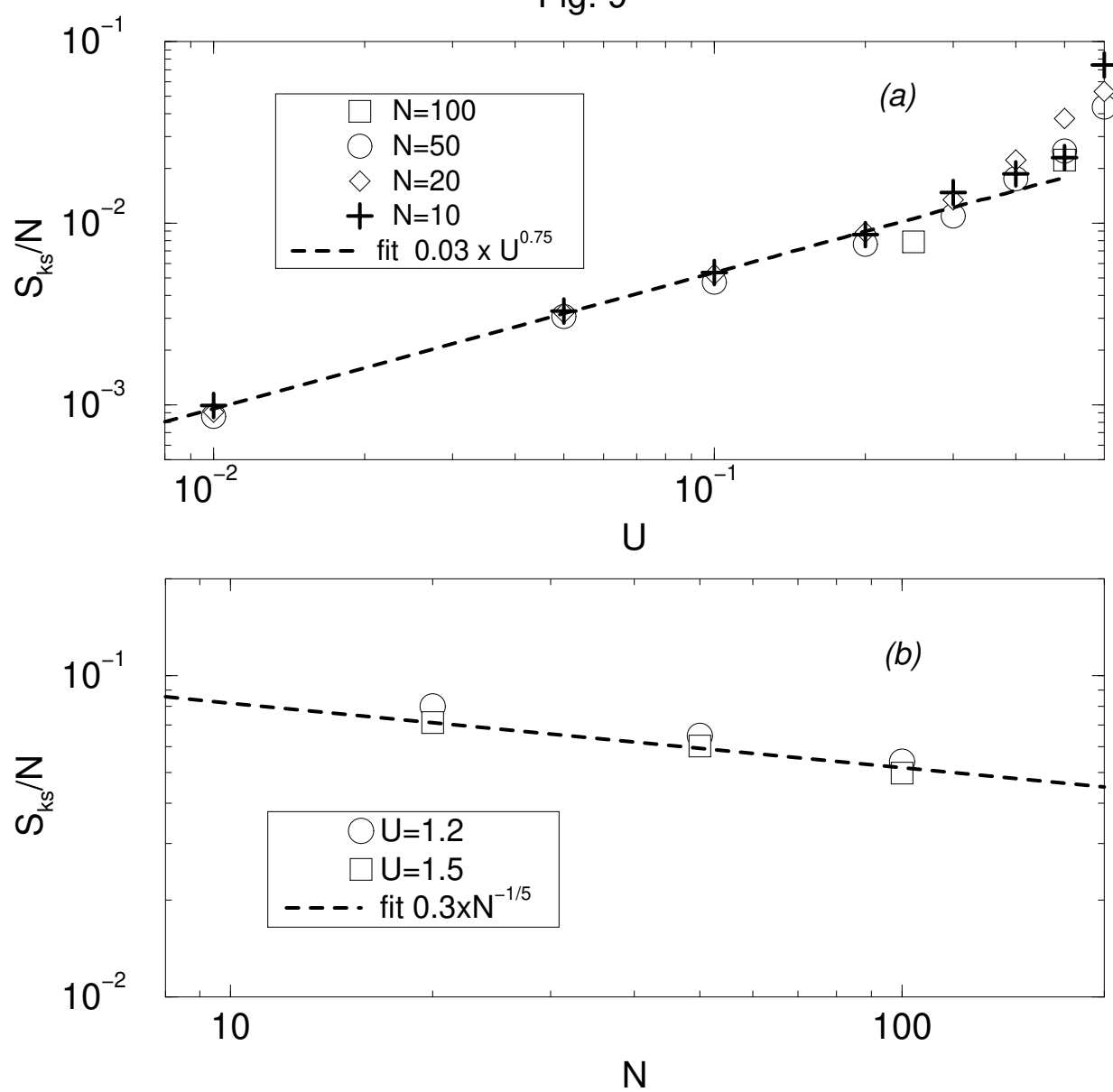


Fig. 10

